Processing and Application of Ceramics 8 [2] (2014) 69–80
DOI: 10.2298/PAC1402069M

Characterizations of microwave plasma CVD grown polycrystalline diamond coatings for advanced technological applications

Awadesh Kumar Mallik*, Nandadulal Dandapat, Shirshendu Chakraborty, Ashok Kumar Mandal, Jiten Ghosh, Manju Unnikrishnan, Sandip Bysakh, Vamsi Krishna Balla

CSIR - Central Glass & Ceramic Research Institute, 196, Raja S C Mullick Road, Kolkata – 700032, India

Received 4 April 2014; received in revised form 22 May 2014; accepted 31 May 2014

Abstract

Polycrystalline diamond (PCD) coatings ranging from few microns to several hundred microns thickness have been grown by 915 MHz microwave plasma reactor with 9000 W power. The coatings were deposited on 100 mm diameter silicon (Si) substrate from few hours to several days of continuous runs. PCD coatings were made freestanding by wet chemical etching technique. The deposited PCDs were evaluated by X-ray diffraction (XRD), scanning electron microscopy (SEM), Raman spectroscopy, X-ray photoelectron spectroscopy (XPS) for physical characterization and compared with authors' earlier work. Refractive index of 2.41 was obtained at 633 nm wavelength and a maximum of 6.6 $W{\cdot}cm^{-1}K^{-1}$ value for thermal conductivity could be achieved with the grown coatings. The values are well above the existing non-diamond heat spreading substrates, which makes the grown PCDs as candidates for heat spreaders in different technological applications. High refractive index along with translucent nature of the white freestanding PCDs, make them potential candidate for optical windows.

Keywords: *vapour deposition, polycrystalline diamond, structural characterization, surfaces, thermal applications*

I. Introduction

Substrates for heat sink are used in many technological applications, especially in high power and high speed electronics, like high frequency microwave devices, high power switches, high power lasers [1–7] etc. There is so much of heat generation that has to be dissipated for efficient operation of the devices [8]. As the Moore's law is becoming difficult to follow because of the limitation of Si material in terms of handling heat and leakage, in the coming years it is mandatory to find a suitable heat spreader material for packaging as many electronic circuits in as much smaller area. Diamond being highest thermal conductivity material can be an alternative semiconducting material of choice for high temperature operations and for quantum computation [9,10]. Polycrystalline diamond (PCD) coatings have so far been used in various thermal management applications [11–21]. CVD diamond has very high thermal conductivity of 5–13 $W{\cdot}m^{-1}K^{-1}$, depending on the quality of the grown coatings. Cu has the highest conductivity among metals [22]. Table 1 shows thermal conductivity and thermal diffusivity values of different metals, ceramics and composites for potential thermal applications. It clearly indicates that CVD diamond is the best among all the available choices.

Since diamond has conductivity well above any existing material it is difficult to measure their thermal properties by available conventional techniques. There have been several methods with certain percentages of margin of error for measuring thermal conductivity [23–43]. Other than heat-spreaders, PCD coatings can also be used as optical windows because of its wide transparency spectrum (ultra violet to microwave). It can also be used in chemical cells for its chemical inertness to most of the acidic and basic reagents.

In the present work, thick PCD coatings were grown by microwave plasma CVD (MWPCVD) process as already reported by the authors [44,45]. The grown coatings were made freestanding following their earlier procedures [46]. In this microwave plasma enhanced CVD process comparatively lower frequency of 915 MHz and

* Corresponding author: tel: +91 33 24733476
fax: +91 33 24730957, e-mail: *amallik@cgcri.res.in*

Table 1. Thermal property comparison of different materials

Material	Thermal conductivity [$W \cdot m^{-1}K^{-1}$]	Thermal diffusivity [cm^2/s]
Pure Mo, pure W	~ 160	0.54
Pure Cu	393	1.11
Pure Al	238	0.84
Cu-W, Cu-Mo alloys	220	-
AlN ceramics	285	1.47
Al-SiC, Cu-Al-SiC, Si-SiC ceramic metal composites	200	-
Single crystal diamond	2000	3–11
CVD diamond	300–1700	1–6
Diamond-Cu composite	550	-

a moderately low power have been used. The novelty of the process lies in the fact that only 8–10 kW of microwave power had been used for diamond growth over large area. In their earlier work, authors had described the MWPCVD process and tuning of the 915 MHz microwave reactor for optimised diamond growth. In previous reports, the thermal properties of the grown coatings were not characterized. Here, the thermal conductivity and diffusivity of the PCD coatings are being reported with corresponding microstructural characteristics. The grown PCDs were further characterized by using scanning electron microscopy (SEM), X-ray diffraction (XRD), Raman spectroscopy, X-ray photoelectron spectroscopy (XPS) for their physical property evaluation and compared with the already published data. The thermal properties were measured by laser flash technique for evaluating their potential application in heat-spreader or other optical application as PCD plates and foils.

II. Experimental

One microwave plasma enhanced chemical vapour deposition (MWPECVD) reactor (Diamotek 1800, Lambda Technologies Inc. USA) has been used for diamond growth as described elsewhere [44,45]. The reactor parameters were varied and optimised [44] to grow two varieties of polycrystalline diamond (PCD) material. The present PCD sample processing conditions are described in Table 2. The grown coatings were made into freestanding material for possible membrane application for heat-sink or any optics [46]. As-grown surface roughness of the samples was measured by coherence scanning interferometry (CSI - Contour GT-K, Bruker Nano GmbH, Germany). Scanning was performed over 0.88 mm × 0.66 mm surface area with 10× objective lens. Back scan and length parameters were 35 μm and 70 μm, respectively. Scanning electron microscope (SEM, LEO 430i Steroscan, UK) was used to see the surface morphology as well as the cross-sectional features. Growth rates were calculated for each case from determination of thickness over definite deposition period. Raman spectroscopy (STR500, Cornes Technologies, formerly known as Seki Technotron) was used to evaluate the coating quality in terms of the amount of diamond to non-diamond deposition. 514.5 nm Ar^+ ion green laser was used with 50 mW power. The Raman signals were taken over 10 seconds of exposure time with 2 times of data acquisitions, using 1200 grating size and 50× objective lens of the spectrometer. Intrinsic stresses of the films in GPa were calculated from the Raman signals with the formula, $\gamma = -0.567 \cdot \Delta\upsilon$, where $\Delta\upsilon$ is the peak shift in cm^{-1} [47]. Minus sign was used to incorporate compressive and tensile nature of the stress present. Moreover the amount of diamond to non-diamond deposition was estimated by quality factor, $Q = I_d/(I_d + I_{glc}) \cdot 100$ (%), where I_d and I_{glc} are the Raman peak intensities for diamond and graphite like carbon, respectively [48]. X-ray diffraction (XRD) (PW 1710, Philips Research Laboratory, Eindhoven, The Netherlands) patterns with Cu-Kα radiation (45 kV, 35 mA) were also recorded for the grown coatings. X-ray photoelectron spectroscopy (XPS) was carried out with a PHI 5000 Versaprobe II scanning XPS microprobe manufactured by UL-VAC PHI, USA, customized for CSIR-Central Glass and Ceramic Research Institute. Details about the instrument can be found from recently published literature [49]. Thermal diffusivity and conductivity were measured by laser flash technique at diamond materials laboratory at

Table 2. Microwave plasma CVD growth parameters of PCD samples

Sample	Time [h]	H_2 flow rate [sccm]	CH_4 flow rate [sccm]	Pressure [Torr]	MW power [kW]	Probe [cm]	Short [cm]	Stage [cm]	Substrate centre temperature [°C]
W1	12.5	850	25.5	118	9.3	8.7	58.6	0.9	1000–1080
	21.5	500	15	118	9.3	8.7	58.6	1	920–1140
W2	66	500	15	118	9	8.7	58.6	1	920–1060
W3	96	500	15	118	9	8.7	58.6	1	900–1140
W4	140	500	15	118	9	8.7	58.6	1	900–1110

General Physics Institute RAS, Moscow. One 1064 nm wavelength Nd-YAG solid state laser with pulse energy of 75 mJ was used to heat one side of the diamond sample, whereas propagation time of the generated heat wave to the opposite side was detected by measuring the temperature with HgCdTe infrared detector with 300 ns operating speed. The thermal measurements were done at room temperature only. Prism coupler (2010/M, Metricon Corporation, USA) was used for recording refractive index of the samples.

III. Results and discussion

3.1. Microwave plasma CVD of diamond

Black quality thick PCD coatings were grown by microwave plasma CVD process as described in Table 2. The coatings were grown over almost identical processing conditions. The sample W1 was deposited over 34 hours duration with an intermediate break after 12.5 hours running, with a change over from 850 sccm to 500 sccm flow rates of hydrogen gas, keeping $CH_4 : H_2$ ratio constant at 3%. The substrate temperature variation was from 1000–1080 °C when hydrogen gas was flowing at higher rates but as the total gas flow rates were brought down from 875.5 sccm to 515 sccm, the substrate surface temperature variation got enhanced across the 100 mm diameter silicon wafer surface, varying from 920–1140 °C. Such a wide temperature distribution across the 4 inch diameter wafer samples W2, W3 and W4 was also noticed during other deposition runs under similar processing parameters for MWCVD. The reason may be the corresponding change in the stage height. The samples W1, W2, W3 and W4 were kept on the water cooled stage during MWPCVD. Silicon substrates were heated only by microwave plasma as there was no additional substrate heater present under the stage. So by suitable adjustments of microwave antenna (probe) and the length of the microwave cavity (distance between stage and short), a hemispherical plasma was generated inside the vacuum chamber. Now the shape and volume of the plasma ball depend on the respective positions of probe, short and height. It was noticed that when the deposition run was interrupted for W1 sample after 12.5 hours, to decrease the hydrogen flow rate, the plasma ball became smaller in volume. So in order to cover the entire 100 mm diameter of the silicon wafer surface area, the stage height was reduced from 1 cm to 0.9 cm, which resulted in regaining full substrate surface coverage of the hemispherical plasma ball. But, it was observed that such change in stage height also affected the wide temperature distribution across the 100 mm diameter surface of the substrate. Since for the sample W1, both the hydrogen gas flow rates and the stage height were altered, it could not be concluded, that which affected the corresponding wide temperature variation. So in the later cases, i.e. for W2, W3 and W4, the hydrogen and methane gas flow rates were kept same as was for the sample W1 deposition condition after interruption. But in all the later cases similar trend in wide temperature variation was noticed. So it was decided to reduce the microwave input power from 9300 to 9000 W. But reduction in input heating energy may have only decreased the limits of upper and lower temperature limits of such temperature variations for the samples W3 and W4. It was observed that such reduction in microwave input power could not prevent temperature to vary as widely as by 240 °C from point to point on the substrate surface. So it may be inferred that the high gas flow rates are essential for uniform temperature distribution. Authors have thoroughly presented their findings about tuning of microwave reactor parameters for establishing temperature uniformity across the silicon substrate surface [44]. In another paper [45] they have presented the optimisation of microwave plasma CVD process for growing large area PCD coatings. The same coating investigated earlier [45] have been used here for comparing the black quality coatings (Table 1) with translucent white free-standing PCD coatings. White coatings were grown using 1000 sccm flow rates at 2% CH_4 to H_2 gas flow ratio.

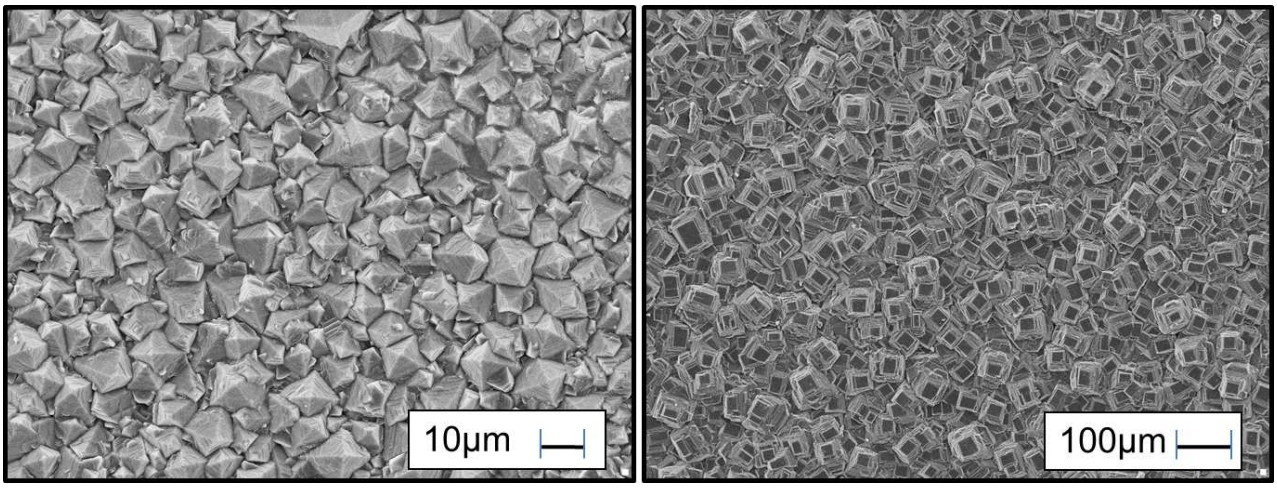

(a) (b)

Figure 1. SEM images showing diamond: a) octahedral and b) cubic crystals

Table 3. Physical properties of the PCD samples: diamond peak intensity (I_d), graphite-like-carbon peak intensity (I_{glc}), quality factor ($Q = I_d/(I_d + I_{glc}) \cdot 100$), diamond peak shift ($\Delta\upsilon$), stress ($\gamma = -0.567 \cdot \Delta\upsilon$), full width at half maximum (FWHM), grain size, roughness, thickness and growth rate

Sample	Raman Spectroscope						Scanning Microscope			
	I_d	I_{glc}	Quality Q [%]	$\Delta\upsilon$ [cm^{-1}]	Stress [GPa]	FWHM	Grain size [μm]	Roughness [μm]	Thickness [μm]	Growth rate [μm/h]
W1	2307	750	75.46	3.2	1.81	15.49	11.7	2.84	79.06	2.32
W2	2430	597	80.27	2.56	1.45	15.99	14	2.61	136.64	2.06
W3	26333	3955	86.94	1.07	0.60	10.29	38.4	9.644	282.45	2.94
W4	3125	971	76.29	1.3	0.73	10.98	12.5	7.06	299.64	2.14

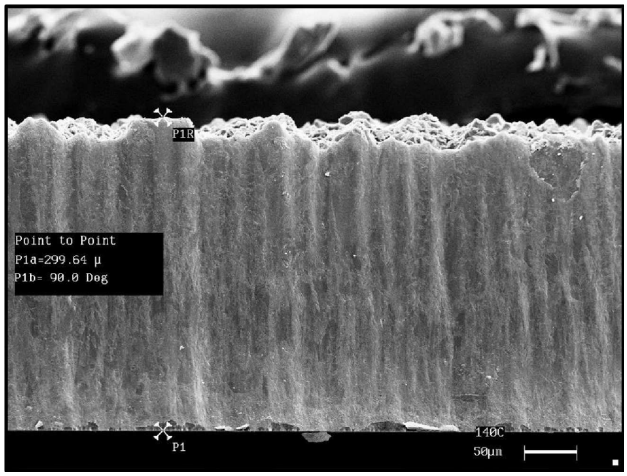

Figure 2. Cross sectional SEM image showing columnar growth structure of CVD diamond for W4 sample

Since to produce whiter variety of coatings a higher total gas flow rate of 1020 sccm was utilised, there was very minimum temperature spread of only 100 °C across the 100 mm diameter substrate surface area.

3.2. As-grown diamond surface morphology - SEM, CSI, XRD

This wide spread in temperature across the substrate surface regions have resulted in varied microstructure of the as-grown PCD coatings. Figure 1a shows the dense octahedral pyramids observed under scanning electron microscope for the sample W1, whereas cubic pyramids were noticed at some surface points for the sample W2. The crystal sizes varied from 11 μm to 38 μm for samples as detailed in Table 3. It is interesting to note that the grain sizes are within 11–14 microns for the samples W1, W2 and W4, but the sample W3 has grain sizes almost four times larger. The sample W3 was deposited over 96 hours of deposition whereas other samples W1 and W2 were deposited for lesser hours of deposition. It was expected that with increase in hours of deposition the crystal sizes will become bigger and bigger, but for the sample W4, although it has the highest hours of CVD growth time, the resultant average grain sizes are not greater than the sample W3 (grown over 96 hours), but it has much lesser value of 12.5 μm. Now if this result is compared with our earlier reported samples [45], we could see that it had average grain size value in between 8–9 μm, which is comparable to W1, W2 and W4 but not at all matching with W3 grains. It is to be noted that the samples from the previous paper were grown over 80 and 116.5 hours of deposition. This abrupt change in grain size for the sample W3 may be due to the cubic pyramids that have grown during CVD process, whereas for other samples the (111) facets of the diamond pyramids are visible. The thicknesses of the samples were measured under cross sectional scanning electron microscopy which revealed columnar structures of the CVD diamond coatings as shown in Fig. 2. If we look at the bottom layer of the cross-sectional SEM micrograph, we could notice that there are distinct individual crystallites with random orientations. Columns start to grow over these randomly oriented crystallites, once they coalesce with each other. The vertical direction growth occurs along the fastest growing planes prevalent among the crystals and the resultant as-grown surface has very high surface roughness due to difference in heights of the growing columns.

These as-grown surfaces, embedded with cubic, cubo-octahedron and octahedron crystals were scanned with a laser surface profilometer. Figure 3 shows the typical micrographs of CSI scans. It can be seen that the samples W1 and W2 has comparatively lower roughness (Table 3) in the order of 2–3 μm whereas the samples W3 and W4 have relatively higher values of surface roughness. This roughness arises due to the asperities and valleys present on the as-grown surface of the PCD and again that is reflected from octahedron and cubic crystals present on the top. Since W3 had predominantly (100) flat surface morphology (in the region where the CSI scan was taken over), it was expected that it would give lower roughness value but to the contrary it has relatively high surface roughness, may be due to larger crystal sizes. The CSI scan revealed surface regions over 100 mm diameter wafer surface area, where there are very big abnormally grown diamond single crystals. It is to be noted that the initial surface roughness of the bare silicon wafer was 30 nm. When the black coatings grown during the present study are compared with our earlier published work samples, it can be seen that it has a much smaller *Ra* surface roughness of 1.96 μm (Fig. 3d). Whereas a very high surface roughness was earlier reported, in the order of 3–4 μm, which was further reduced to nanometer level by surface planarization.

The thicknesses of the coatings were then divided by the respective deposition times, giving the growth rate

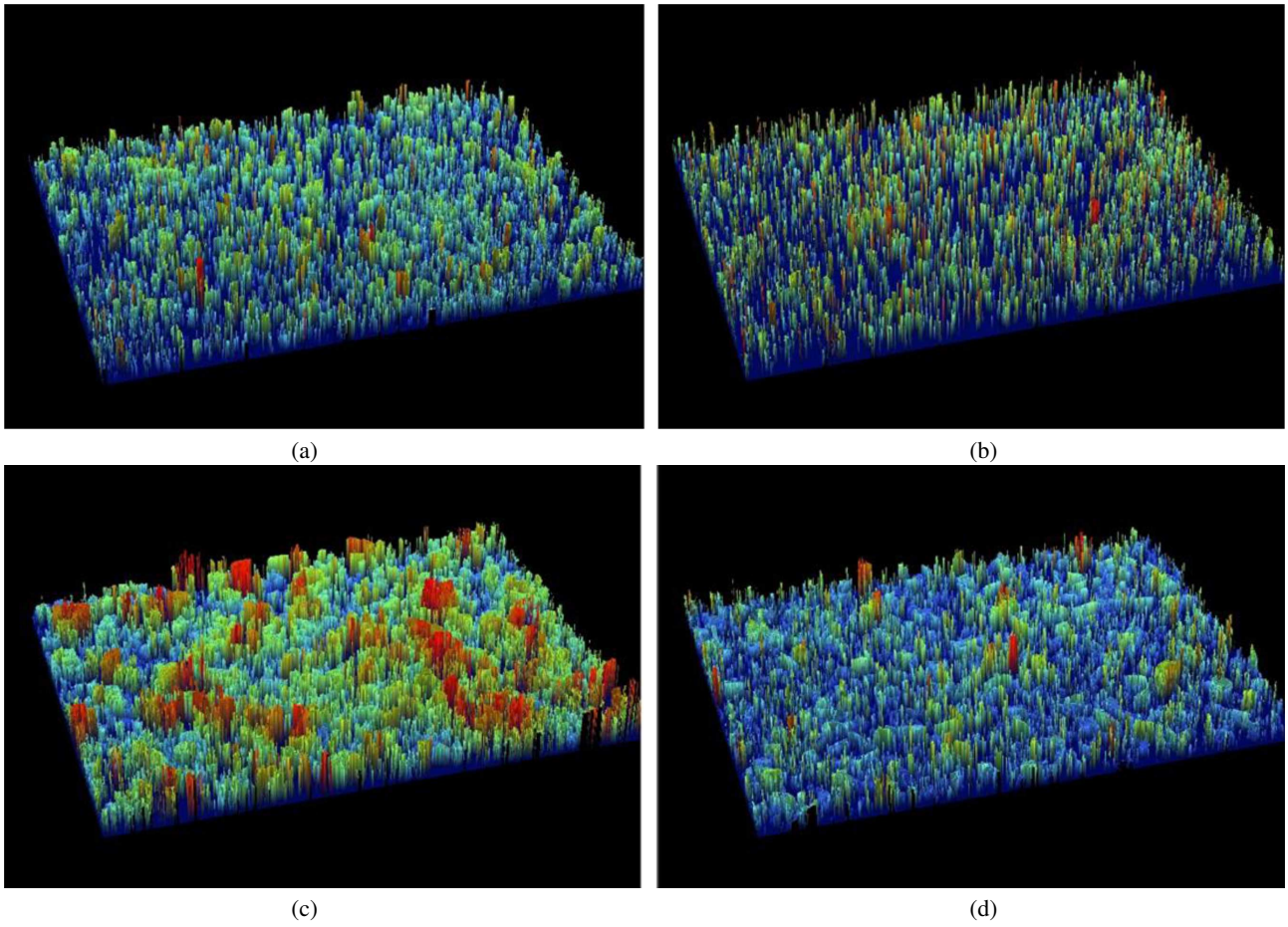

Figure 3. Coherence scanning interferometer surface roughness area scan: a) W1, b) W2, c) W3 and d) white PCD samples

for each sample, as shown in Table 3. Again it could be observed that the growth rates are comparable for the samples W1, W2 and W4, but for the sample W3, growth rate is considerably high. Now, diamond CVD growth rates depend on several processing parameters like pressure, substrate temperature, methane percentages etc. It is well known in the literature [50] that with increase in substrate temperature and methane percentages, the growth rate increases and reaches an optimal value before start decreasing (rather degrading) further. When we compare the present work samples W1, W2, W3 and W4 with our earlier studied samples [45], we can infer that in the present study higher percentages of methane gas results higher growth rate in the order of 2–3 μm/h whereas reported samples [45] had only 1 μm/h of growth rate. Both the values of growth rates are in agreement with reported literature using similar experimental reactor by Zuo *et al.* [51]. The slow deposition rate earlier produced whiter variety of diamond coating whereas all the samples in the present study have black texture. Now, it is to be observed that in our earlier paper, PCD was grown with 2% methane concentration in 1000 sccm of hydrogen flowing gas, whereas in the present work, 3% methane was flown into 500 sccm of hydrogen gas plasma. The effect is twofold: (i) the as-grown PCD becomes darker in texture with more number of defects present inside and, (ii) the substrate surface centre temperature becomes very unstable. In our previous study for the whiter grade PCDs, the temperature remains more stable at 1050 °C, but in the present work we report very wide temperature instability at the centre as well as across the 100 mm diameter silicon substrate surface.

It is well known that CVD diamond growth has a definite temperature window from 700–1200 °C. The growth rate is slow at the lower temperature range and it increases with increasing temperature and then fades out as it reaches higher temperature domain. Now, it may have happened here that the temperature of the substrate surface region, where the SEM micrograph was taken from, for the sample W3, was at the higher temperature suitable for high growth rate, whereas for the samples W1, W2 and W4, the temperature was conducive for moderate growth rate. This may have happened if we consider only the substrate temperature parameter. Growth rate also depends on other factors like chamber pressure, methane percentages, deposition time etc. It is well known that higher methane percentages will result in higher growth rate but at the expense of its quality. This exactly has happened in our present work for changing to 3% of CH_4 concentration in the precursor gas composition. But in authors' earlier reported study a comparatively lower growth rate was achieved, with lower methane percentage and with higher flow rate of

hydrogen. Role of hydrogen is to produce purer PCD crystals and that was exactly the reason behind getting white diamond in our earlier work [45]. Now, if we consider the effect of chamber pressure on the growth rate of diamond, it can be observed that higher pressure leads to higher substrate temperature for microwave plasma CVD and also it enhances the growth rate. There is a pressure window where the growth rate is linear with pressure but after 120 Torr of chamber pressure it has been reported to increase exponentially the growth rate before attaining saturation value [50]. In the present case the used chamber pressure was 118 Torr which is slightly below the pressure value where exponential rise of growth occurs. So it could not be observed any rapid rise of diamond deposition rate with time. In our earlier study, still lower pressure of 110 Torr was used, which may be another reason of getting further lower growth rate for the white PCDs. Deposition time plays very important role in determining the thickness of the PCD. As it is known that initially the thickness does not increase much due to nucleation and growth of diamond colonies on the substrate surface, once they coalesce with each other, the thickness increase rapidly to give definitive texture to the film, perpendicular to the substrate surface. Once texture has been formed the thickness increase uniformly with almost constant growth rate.

Important parameter in determining growth rate is the residence time of the precursor gases inside the deposition chamber. For a given chamber volume and with constant precursor gas flow rates, the residence time increases with chamber pressure. So if 515 sccm of methane hydrogen gas mixture is fed into 5 litre vacuum deposition chamber at 118 Torr, then the estimated residence time is about 1.5 minute. On the other hand in our earlier work [45], the total gas flow rate was 1020 sccm inside the same 5 litre chamber at 110 Torr, giving rise to a residence time of 43 seconds, approximately. As long as the gases are present inside the vacuum chamber, they are undergoing chemical reactions, leading to deposition of diamond. The amount of carbon that gets converted into diamond during residence time inside the reaction chamber is the carbon conversion efficiency. It is expected that lower flow rates will lead to higher residence time thus giving rise to higher carbon conversion to diamond, sometimes with co-deposition of non-diamond phases with degradation of overall quality. Now the samples W1, W2, W3 and W4 were grown with higher residence time compared to the previous work [45], and higher carbon conversion efficiency has led to secondary nucleation of the grown PCDs (Fig. 4a). Such high residence time has degraded the overall PCD quality in terms of crystal defects and Raman signals (Fig. 5). Secondary nucleation sites also define the diamond film quality. It is noticed that as the growth rate increases, the points of secondary nucleation also increases, leading to poorer quality of diamond films (sometimes cauliflower like morphology, but was not observed in the present case). So to get a higher quality film it is desired that hydrogen flux has to be higher to clean the as-grown diamond surface from non-diamond deposition and also lower percentages of methane to be used to avoid secondary nucleation. The X-ray diffraction peaks (Fig. 4b) for all the samples have reflection peaks from (111) planes with additional peak from (220) plane. The texture of the film is determined by the fastest growing direction perpendicular to the substrate surface. After the initial nucleation and surface coverage period, the fastest growing direction outfast other growth direction along the perpendicular direction to the substrate surface. Once the texture has been formed (fastest growing crystal direction perpendicular to the surface) the diamond surface morphology is defined by the slowest growing planes. The diamond film morphology depends on the preferential growth of different planes along different directions. It is well known [50] that diamond crystals grow fastest along [111] directions to give cubic crystals and when the growth rate along [100] direction is the high-

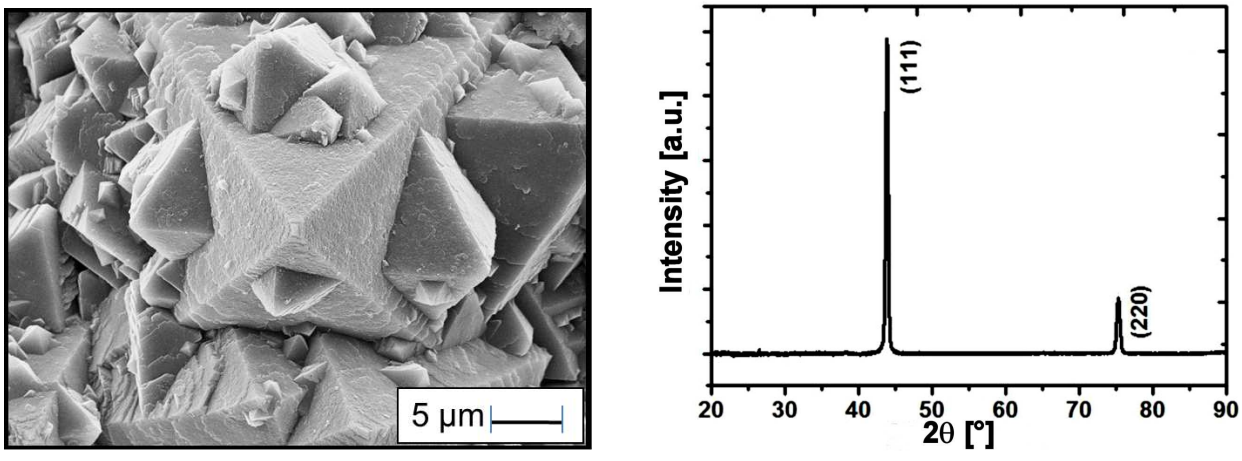

(a) (b)

Figure 4. Secondary nucleation on the side surfaces of diamond octahedral (a) and typical X-ray diffraction pattern for present work PCD samples (b)

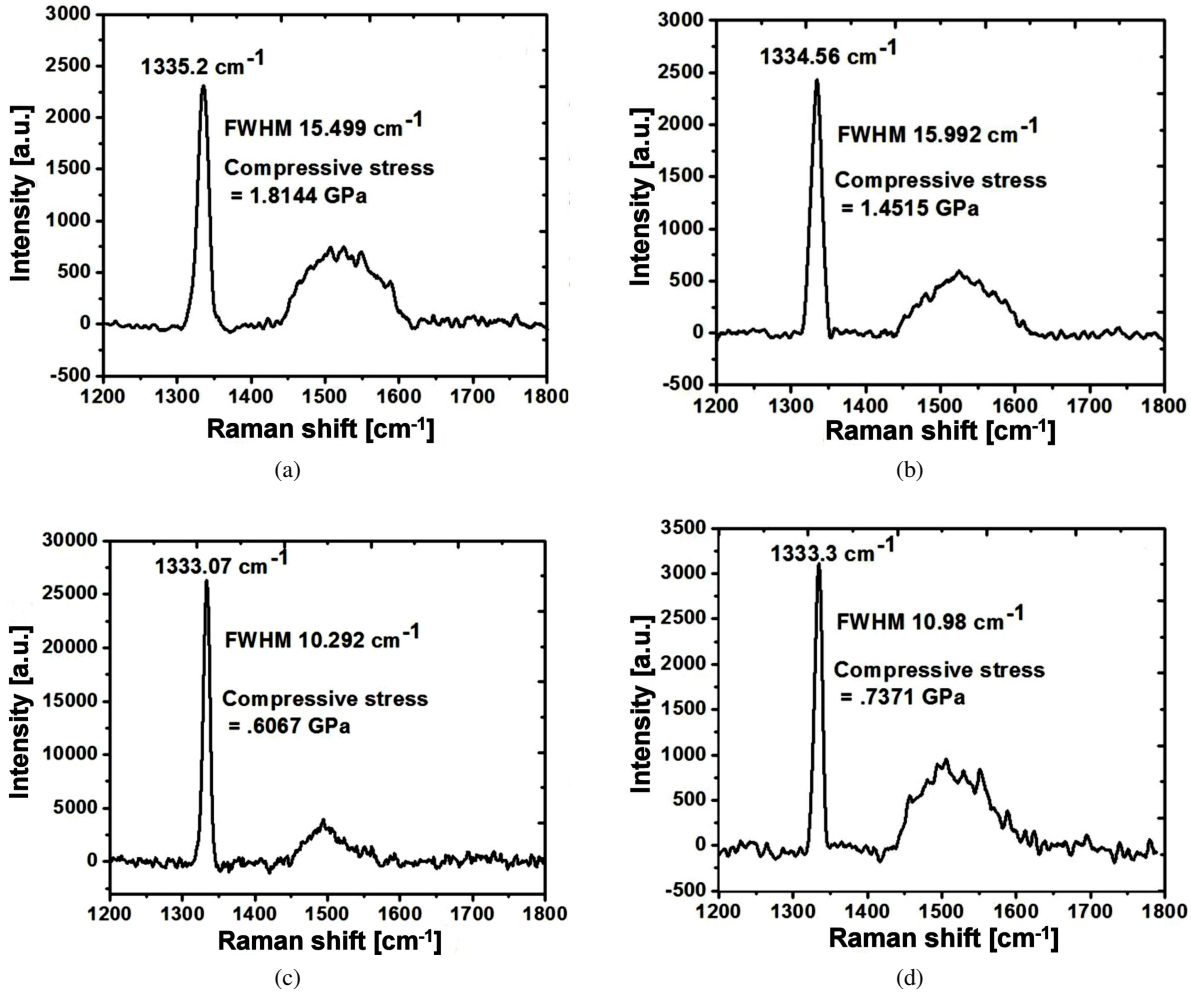

Figure 5. Raman signals for: a) W1, b) W2, c) W3 and d) W4 PCD samples

est with preferential growth of (100) planes, the resultant crystal morphology is octahedron, surrounded by (111) planes. Any intermediate growth rates give rise to cubo-octahedron crystals. The ratio of growth velocities along [100] and [111] directions can be expressed as α parameter. It has been shown that when α parameter is close to 1, the atoms grow faster along [111] directions giving rise to cubic crystals of diamond as shown in Fig. 1b. On the other hand, when the faster growth direction is [100], the resultant crystals are surrounded by (111) planes with octahedral diamond crystals (Fig. 1a) for α value close to 3. Any intermediate α parameter value gives rise to cubo-octahedral crystals. Higher substrate temperature decreases α parameter, i.e. it promotes cubic morphology ([111] fastest direction and (100) slowest growing planes). On the other hand, with higher methane percentages, the diamond surface morphology is octahedron with α parameter close to 3 (i.e. [100] fastest growing direction and (111) slowest growing planes). In the present case the samples W1, W2 and W4 have octahedron morphology which can be correlated with lower substrate temperature and higher methane percentages. But W3 has cubic morphology indicating a comparatively higher temperature of deposition and may have low methane percentages. Also literature [52] on diamond surface morphology reported evolution of (111) to (100) to secondary nucleated microcrystals as the methane percentages are increased gradually. But here CH_4 gas flow rates were constant for all the samples. So it can be concluded that the reason behind formation of cubic crystals may be very high substrate surface temperature at the point of measurement under scanning electron microscope. In our earlier published results [44], it has been shown that how the substrate temperature varies widely across the 100 mm diameter silicon substrate surface, and it was also observed that efficient tuning of the reactor parameters helped in achieving better thermal management for CVD diamond growth. In the present case, citing earlier work report [53], it can be inferred that cubic morphology and abnormality in substrate temperature was responsible for such anomaly in results for as-grown region of study for the sample W3.

3.3. As-grown diamond surface quality - Raman, XPS

If we look at the Raman signals (Fig. 5) from these samples it can be found that the diamond peaks are present with some shifts from theoretical *sp3* peak

position of 1332 cm^{-1}. As the samples were made free-standing, it can be said that these shifts are due to intrinsic stress present in the film due to CVD processing. The FWHM values are quite high showing the inferior quality of the coatings. It is the convention that FWHM greater than 12 cm^{-1} to be counted as poor quality diamond and coatings with less than 12 cm^{-1} FWHM values are considered purer quality coating. Going by this standard, it can be stated that W1 and W2 are bad in quality compare to W3 and W4 PCD samples. Whereas, our earlier reported samples [45] had only 3.6 cm^{-1} FWHM, showing high quality white grade diamond deposition. Another quantitative way of assessing the quality of the PCDs is by calculating percentage ratio of the diamond to non-diamond content of the coatings. The Raman peak position shift, intrinsic stress and quality have been tabulated and are shown in Table 3 and Fig. 5. It is to be noted that the best signals were obtained from the sample W3 with the best quality factor ratio (~87%) and the least compressive stress (−0.6 GPa). The reason behind such a good quality can be attributed to its bigger grain size (~38 μm). The Raman signals were taken using confocal microscope with 50× objective lens giving a 5 μm laser spot size. Now, the grain sizes of W1, W2 and W4 are in the order of 10 micron which is very likely to include grain boundary during Raman signal acquisitions, whereas the large grain size of the sample W3 might have avoided grain boundary region signal acquisitions, which is the reason behind high intensity signals from the sample W3 (Fig. 5c). Moreover, the intrinsic stress value is also the lowest for W3 among others. This can be attributed to low defect density in large PCD crystals but this result is in contradiction to another highest value for W3, i.e. its growth rate. So it is important to understand the growth mechanisms present in W3 in comparison to the others.

Figure 6 describes the typical growth features observed in W3 and other samples. It is to be seen that the W3 crystals are formed by stacking of successive (100) facets (Fig. 6b) whereas crystals of other samples have (111) surface morphology (Fig. 6a). (111) planes become evident (Fig. 6a) as (100) planes are stacked upon each other with [100] as the fastest direction. On the other hand, (100) facets are evident (Fig. 6b) for W3 in the growing surface when the (111) planes stack upon each other along [111] direction to produce cubic morphology. It can be seen that such cubic crystal surfaces are embedded with spiral growth features (even was visible under CSI scan and optical microscope). The surface temperatures for the sample W3 were so abnormally distributed that we noticed at some locations very large diamond single crystals (abnormal grain growth) as shown in Fig. 6c. Such crystals were square in shape and somewhere as big as 300 μm in size. Under optical microscope, spiral growth features were observed on the top surface of such big single crystals, along with twinning. On the other hand, octahedrons crystal growth is characterized by side surface step-wise pyramidal structures (Fig. 6a).

So far it has been observed that there are two varieties of the as-grown PCD samples. One set of samples have characteristic black texture and the authors' earlier reported sample had white texture (Table 4). It has also been seen that the black samples are of inferior quality to the whiter variety of diamond samples. So, it was essential to characterize the elements present on the black and white diamond surfaces. X-ray photoelectron spectroscopy was done for the W3 (being of special nature) and white PCD samples (supply from paper [45]). Figures 7c,f are the O1s binding energies for oxygen contaminated diamond surface at the theoretical peak position of 531 eV and all the spectra are aligned with respect to this O1s binding energy position. Figures 7a,d show the survey scan for detecting elements on the surface of the as-grown PCDs. Diamond surface was not devoid of oxygen as the samples were kept outside, under atmospheric condition, after taking out from microwave plasma CVD chamber and before putting inside XPS vacuum chamber. Theoretical position of C1s peak is at 284.4 eV for CVD diamond [54] and Fig. 7a shows a downshift in peak positions by 1.4 eV for black grade diamond and Fig. 7d shows an upshift in peak position by 0.2 eV for white grade diamond respectively. Moreover, it can be found that the intensity of O1s peak is less for black grade diamond in comparison to white grade PCD sample. This implies that the fresh diamond surface is more susceptible to oxygen absorption under atmosphere for white diamond than its darker variety. The reason may be *sp3* carbon in the white diamond sample which adsorbs more oxygen than con-

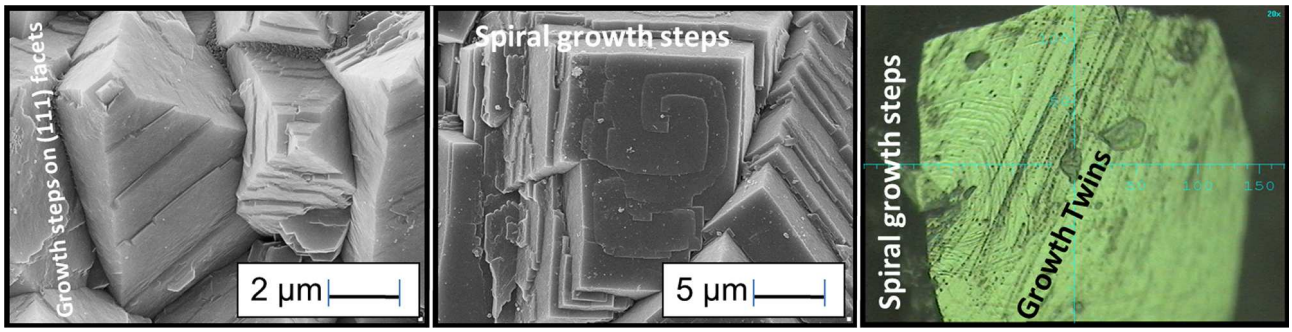

Figure 6. SEM micrographs showing growth features for: a) octahedral and b) cubic crystals and c) optical micrograph for growth features of abnormally grown 300 μm square crystals

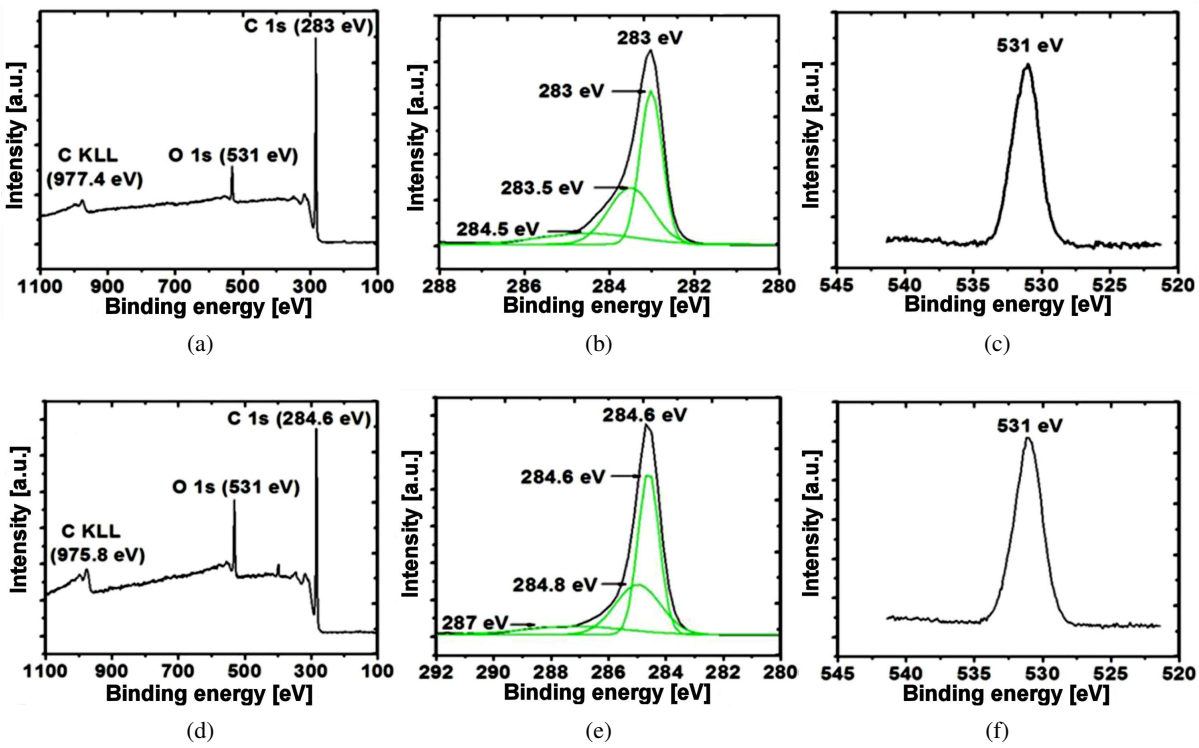

Figure 7. XPS signals for black diamond samples: a) wide surface scan, b) C1s and c) O1s, and for white diamond samples: d) wide surface scan, e) C1s and f) O1s

taminated variety of the darker samples. In other words, purer diamond surface has more dangling bonds to adsorb atmospheric oxygen than the less pure diamond, where the surface might be contaminated with graphitic and amorphous carbon structures, which do not have as many unsaturated surface bonds as pure diamond surface to adsorb oxygen. Now, when individual C1s peaks are analysed for both the grades of PCDs, it is seen that the individual C1s peak can be de-convoluted into three separate peaks. It is known from the literature that amorphous carbon and graphite phase give XPS peaks at 284.4 eV and 284.3 eV, respectively, which are unfortunately coinciding with theoretical binding energy values for diamond films. Now, in the present study, for both varieties of diamond there are three deconvoluted C1s peaks, each of which may correspond to diamond, amorphous carbon and graphitic inclusion in the as-grown PCDs. So it can be concluded that XPS can not be termed as phase identifying characterization tool for CVD diamond samples. But the C1s peak can indicate the extent of contamination of the diamond sample. Figure 7b,e shows the presence of all forms of carbon without pointing out definite phase but from the highest peak intensities it can be inferred that the binding energy for diamond phase correspond to 283 eV for the black grade and 284.6 eV for the white variety of diamond.

3.4. Diamond thermal and optical properties

In order to measure the thermal properties of the white and black grade diamonds, it was necessary to cut the samples into desired geometrical shape and size. The thicker black grade sample was cut into 12.5 mm circular discs and the whiter samples were cut into 40 mm circular plates by 1064 nm Nd:YAG solid state 10 W laser under open atmosphere. The thickness was again measured directly by a screw gauge, as well as from mass and size of the sample. It was found that the two thicknesses differ largely. This difference can be attributed to inherent porosity in the thin film structure introduced during CVD process. While calculating thermal diffusivity and conductivity, the thickness obtained from mass, was used. The thickness measured by a gauge was too high because of high surface roughness (and a curvature of the plates). It was found that when the PCD was adhered to the base silicon substrate, the surface was flat and parallel. But it was due to strong bonding between the substrate and the coating. Since sili-

Table 4. Physical property comparison of black and white PCD samples: diameter of circular plate (D), weight in Carat, thickness, thermal diffusivity ($D_\perp$), thermal conductivity ($k_\perp$)

Polycrystalline diamond sample	D [mm]	Weight in Carat	Thickness (from mass) [μm]	Thickness (gauge) [μm]	$D_\perp$ [cm^2/s]	$k_\perp$ [W·cm^{-1}K^{-1}]
Black, opaque	12.5	0.347	161	200	3.5	6.3
White, translucent	40	1.73	78	90	3.7	6.6

con and diamond has different co-efficient of thermal expansion, the as-grown PCD coatings remain under compressive stress once the CVD processing temperature comes down from 1000 °C to the room temperature. It has been observed that when the PCD is made freestanding from the base silicon substrate, the diamond plates or foils have some curvature left within. But here, the resultant error (±15%) in the thermal conductivity measurements is mainly due to the uncertainty in film thickness. Density of diamond was used 3.51 g/cm^3 and the heat capacity was taken 0.51 J·g^{-1}K^{-1} during calculations. Thermal diffusivity was measured to be 3.5 cm^2/sec for the black diamond, whereas, the white diamond gives 3.7 cm^2/sec thermal diffusivity (Table 4). It was again found that the thermal conductivity of the black type of PCDs is marginally less than that of the white variety diamond. All these thermal property values correspond to perpendicular to the surface of the diamond plates, not their in-plane results. Reported literature values of thermal conductivity for CVD grown diamonds vary from 5–20 W·cm^{-1}K^{-1}. In the present study the coatings fall in the lower range of the reported values available from other research papers. But such values of 6 W·cm^{-1}K^{-1} or more, is well above any other available metal, ceramic or composite material (Table 1). Thus, these freestanding diamond coatings can be used for potential heat spreader application for thermal management. Moreover, these freestanding plates have found to be translucent in case of the whiter grades PCDs with very high refractive index of 2.41 [46]. But the black colour coatings are completely opaque in nature so it has limitations for thermal management applications or any biological applications. Whereas, the white grade diamond plates can be used in high power optics for transmission windows.

IV. Conclusions

Polycrystalline diamond films have been grown by microwave plasma CVD. The as-grown coatings have varied microstructure from perfect octahedral to perfect cubic crystals. This wide range of surface morphology was due to wide variation of surface temperature of the silicon substrate. The cubic crystals were grown with spiral growth features on the surface and the octahedrals were grown with stepwise side growth surface. The intermediate microstructures of cubo-octahedrals are embedded with secondary nucleation crystals on the side surfaces. Abnormality in surface temperature distribution also results in abnormal crystal growth. Raman and XPS results show that better quality coatings can be grown with higher amount of hydrogen gas with low methane percentages. Such whiter grade coatings have much better thermal and optical properties, suitable for many technological applications as freestanding diamond plates, whereas the darker variety PCDs can only be used for thermal applications.

Acknowledgement: The present work was financially supported by CSIR, India under 12th Five Year Plan network project titled “Microwave tube - design and development capabilities (MTDDC)”, Grant no. PSC 0101. Dr. Victor Ralchenko provided the thermal conductivity and diffusivity results of the diamond samples. Dr. Kaushik Biswas kindly did the optical property measurements.

References

1. P. Millar, A.J. Kemp, D. Burns, “Power scaling of Nd:YVO_4 and Nd:$GdVO_4$ disk lasers using synthetic diamond as a heat spreader”, *Opt. Lett.*, **34** [6] (2009) 782–784.
2. H. Lindberg, A. Larsson, M. Strassner, “Single-frequency operation of a high-power, long-wavelength semiconductor disk laser”, *Opt. Lett.*, **30** [17] (2005) 2260–2262.
3. Y. Kim, S. Cho, S.-M. Lee, G.B. Kim, J. Lee, J. Yoo, K.-S. Kim, T. Kim, Y. Park, “Highly efficient green VECSEL with intra-cavity diamond heat spreader”, *Electron. Lett.*, **43** [2] (2007) 1–2.
4. B. Rudin, A. Rutz, M. Hoffmann, D.J.H.C. Maas, A.-R. Bellancourt, E. Gini, T. Südmeyer, U. Keller, “Highly efficient optically pumped vertical-emitting semiconductor laser with more than 20 W average output power in a fundamental transverse mode”, *Opt. Lett.*, **33** [22] (2008) 271–272.
5. H. Lindberg, M. Strassner, E. Gerster, A. Larsson, “0.8W optically pumped vertical external cavity surface emitting laser operating CW at 1550 nm”, *Electron. Lett.*, **40** [10] (2004) 1–2.
6. M. Butkus, K.G. Wilcox, J. Rautiainen, O.G. Okhotnikov, S.S. Mikhrin, I.L. Krestnikov, A.R. Kovsh, M. Hoffmann, T. Südmeyer, U. Keller, E.U. Rafailov, “High-power quantum-dot-based semiconductor disk laser”, *Opt. Lett.*, **34** [11] (2009) 1672–1674.
7. A. Harkonen, S. Suomalainen, E. Saarinen, L. Orsila, R. Koskinen, O. Okhotnikov, S. Calvez, M. Dawson, “4W single-transverse mode VECSEL utilising intra-cavity diamond heat spreader”, *Electron. Lett.*, **42** [12] (2006) 693–694.
8. P.K. Schelling, L. Shi, K.E. Goodson, “Managing heat for electronics”, *Mater. Today*, **8** [6] (2005) 30–35.
9. H. Bernien, H.B. Hensen, W. Pfaff, G. Koolstra, M.S. Blok, L. Robledo, T.H. Taminiau, M. Markham, D.J. Twitchen, L. Childress, R. Hanson, “Heralded entanglement between solid-state qubits separated by three metres”, *Nature*, **497** (2013) 86–90.
10. J. Wolters, M. Strau, R.S. Schoenfeld, O. Benson, “Study of the quantum zeno phenomenon on a single solid state spin”, *Phys. Rev. A*, **88** (2013) 020101(R).
11. K. Jagannadham, “Multilayer diamond heat spreaders for electronic power devices”, *Solid-State Electron.*, **42** [12] (1998) 2199–2208.
12. P.W. Juodawlkis, J.J. Plant, L.J. Missaggia, K.E. Jensen, F.J. O’Donnell, “Advances in 1.5-μm InGaAsP/InP Slab-Coupled Optical Waveguide Amplifiers (SCOWAs)”, pp. 309–310 in *The Proceed-*

ings of The 20th Annual Meeting of the IEEE, Lasers and Electro-Optics Society, LEOS 2007.
13. H. Lindberg, M. Strassner, A. Larsson, "Improved spectral properties of an optically pumped semiconductor disk laser using a thin diamond heat spreader as an intracavity filter", *IEEE Photonics Technol. Lett.*, **17** [7] (2005) 1363–1365.
14. K.S. Kim, J.R. Yoo, S.H. Cho, S.M. Lee, S.J. Lim, J.Y. Kim, J.H. Lee, T. Kim, Y.J. Park, "1060 nm vertical-external-cavity surface-emitting lasers with an optical-to-optical efficiency of 44% at room temperature", *Appl. Phys. Lett.*, **88** (2006) 091107.
15. W.D. Brown, R.A. Beera, H.A. Naseem, A.P. Malshe, "State-of-the-art synthesis and post-deposition processing of large area CVD diamond substrates for thermal management", *Surface Coatings Technol.*, **86–87** [2] (1996) 698–707.
16. P.H. Chen, C.L. Lin, Y.K. Liu, T.Y. Chung, C.Y. Liu, "Diamond heat spreader layer for high-power thin-GaN light-emitting diodes", *IEEE Photonics Technol. Lett.*, **20** [10] (2008) 845–847.
17. C. Lee, J. Ward, R. Lin, E. Schlecht, G. Chattopadhyay, J. Gill, B. Thomas, A. Maestrini, Mehdi, P. Siegel, "A wafer-level diamond bonding process to improve power handling capability of submillimeter-wave Schottky diode frequency multipliers", pp. 957–960 in *Microwave Symposium Digest, MTT '09.* IEEE MTT-S International, 2009.
18. K. Jagannadham, T.R. Watkins, R.B. Dinwiddie, "Novel heat spreader coatings for high power electronic devices", *J. Mater. Sci.*, **37** (2002) 1363–1376.
19. A.V. Sukhadolau, E.V. Ivakin, V.G. Ralchenko, A. V. Khomich, A.V. Vlasov, A.F. Popovich, "Thermal conductivity of CVD diamond at elevated temperatures", *Diam. Relat. Mater.*, **14** (2005) 589–593.
20. A. Rogacs, J. Rhee, "Performance-cost optimization of a diamond heat spreader", pp. 65–72 in *The Proceedings of 12th International Symposium, Advanced Packaging Materials: Processes, Properties, and Interfaces*, APM 2007.
21. J. Bonhaus, D. Borchert, A. Denisenko, W.R. Fahrner, "Diamond heat spreaders for high power devices with integrated temperature sensors", pp. 139–146 in *he Proceedings of the Fourteenth IEEE Semi-Therm Symposium, Semiconductor Thermal Measurement and Management*, IEEE, USA, 1998.
22. K. Yoshida, H. Morigami, "Thermal properties of diamond/copper composite material", *Microelectron. Reliab.*, **44** [2] (2004) 303–308.
23. K.J Gray, "Effective thermal conductivity of a diamond coated heat spreader", *Diam. Relat. Mater.*, **9** [2] (2000) 201–204.
24. D. Francis, F. Faili, D. Babić, F. Ejeckam, A Nurmikko, H. Maris, "Formation and characterization of 4-inch GaN-on-diamond substrates", *Diam. Relat. Mater.*, **19** [2–3] (2010) 229–233.
25. S. Ahmed, R. Liske, T. Wunderer, M. Leonhardt, R. Ziervogel, C. Fansler, T. Grotjohn, J. Asmussen, T. Schuelke, "Extending the 3x-method to the MHz range for thermal conductivity measurements of diamond thin films", *Diam. Relat. Mater.*, **15** (2006) 389–393.
26. J.E. Graebner, V.G. Ralchenko, A.A. Smolin, E.D. Obraztsova, K.G. Korotushenko, V.I. Konov, "Thermal conductivity of thin diamond films grown from d.c. discharge", *Diam. Relat. Mater.*, **5** (1996) 693–698.
27. D.J. Twitchena, C.S.J. Picklesa, S.E. Coea, R.S. Sussmanna, C.E. Hallb, "Thermal conductivity measurements on CVD diamond", *Diam. Relat. Mater.*, **10** (2001) 731–735.
28. H. Verhoeven, J. Hartmann, M. Reichling, W. Müller-Sebert, R. Zacha, "Structural limitations to local thermal diffusivities of diamond films", *Diam. Relat. Mater.*, **5** [9] (1996) 1012–1016.
29. S.E. Coe, R.S. Sussmann, "Optical, thermal and mechanical properties of CVD diamond", *Diam. Relat. Mater.*, **9** (2000) 1726–1729.
30. H. Relyea, M. White, J.J. McGrath, J.V. Beck, "Thermal diffusivity measurements of free-standing CVD diamond films using non-contacting, non-destructive techniques", *Diam. Relat. Mater.*, **7** (1998) 1207–1212.
31. C. Stehl, M. Schreck, M. Fischer, S. Gsell, B. Stritzker, "Thermal diffusivity of heteroepitaxial diamond films: Experimental setup and measurements", *Diam. Relat. Mater.*, **19** (2010) 787–791.
32. A.V. Khomich, V.G. Ralchenko, A.V. Vlasov, R.A. Khmelnitskiy, I.I. Vlasov, V.I. Konov, "Effect of high temperature annealing on optical and thermal properties of CVD diamond", *Diam. Relat. Mater.*, **10** [3–7] (2001) 546–551.
33. K.M. Leung, A.C. Cheung, B.C. Liu, H.K. Woo, C. Sun, X.Q. Shi, S.T. Lee, "Measuring thermal conductivity of CVD diamond and diamond-like films on silicon substrates by holographic interferometry", *Diam. Relat. Mater.*, **8** (1999) 1607–1610.
34. Y. Yamamoto, T. Imai, K. Tanabe, T. Tsuno, Y. Kumazawa, N. Fujimori, "The measurement of thermal properties of diamond", *Diam. Relat. Mater.*, **6** (1997) 1057–1061.
35. E. Wörner, C. Wild, W. Müiller-Sebert, R. Locher, P. Koidl, "Thermal conductivity of CVD diamond films: high-precision, temperature-resolved measurements", *Diam. Relat. Mater.*, **5** (1996) 688–692.
36. K. Plamann, D. Fournier, B.C. Forget, A.C. Boccara, "Microscopic measurements of the local heat conduction in polycrystalline diamond films", *Diam. Relat. Mater.*, **5** (1996) 699–705.
37. E. Jansen, O. Dorsch, E. Obermeier, W. Kulisch, "Thermal conductivity measurements on diamond films based on micromechanical devices", *Diam. Relat. Mater.*, **5** (1996) 644–648.
38. J.E. Graebner, "Simple correlation between optical absorption and thermal conductivity of CVD diamond", *Diam. Relat. Mater.*, **4** (1995) 1196–1199.

39. A.N. Obraztsov, I.Y. Pavlovsky, H. Okushi, H.Watanabe, "Direct measurement of CVD diamond film thermal conductivity by using photoacoustics", *Diam. Relat. Mater.*, **7** (1998) 1513–1518.
40. J.E. Graebner, M.E. Reiss, L. Seibles, T.M. Hartnett, R.P. Miller, C.J. Robinson, "Phonon scattering in chemical-vapor-deposited diamond", *Phys. Rev. B*, **50** [6] (1994) 3702–3713.
41. J.E. Graebner, H. Altmann, N.M. Balzaretti, R. Campbell, H.B. Chae, A. Degiovanni, R. Enck, A. Feldman, D. Fournier, J. Fricke, J.S. Goela, K.J. Gray, Y.Q. Gu, I. Hatta, T.M. Hartnett, R.E. Imhof, R. Kato, P. Koidl, P.K. Kuo , T.K. Lee, D. Maillet, B. Remy, J.P. Roger, D.J. Seong, R.P. Tye, H. Verhoeven, E. Worner, J.E. Yehoda, R. Zachai, B. Zhang, "Report on a second round robin measurement of the thermal conductivity of CVD diamond", *Diam. Relat. Mater.*, **7** (1998) 1589–1604.
42. J.E. Graebner, "Measurements of specific heat and mass density in CVD diamond", *Diam. Relat. Mater.*, **5** (1996) 1366–1370.
43. J.E. Graebner, J.A. Mucha, F.A. Baiocchi, "Sources of thermal resistance in chemically vapor deposited diamond", *Diam. Relat. Mater.*, **5** (1996) 682–687.
44. A.K. Mallik, K.S. Pal, N. Dandapat, B.K. Guha, S. Datta, D. Basu, "Influence of the microwave plasma CVD reactor parameters on substrate thermal management for growing large area diamond coatings inside a 915 MHz and moderately low power unit", *Diam. Relat. Mater.*, **30** (2012) 53–61.
45. A.K. Mallik, S. Bysakh, K.S. Pal, N. Dandapat, B.K. Guha, S. Datta, D. Basu, "Large area deposition of polycrystalline diamond coatings by microwave plasma CVD", *T. Indian Ceram. Soc.*, **72** [4] (2013) 225–232.
46. A.K. Mallik, S. Bysakh, K.S. Pal, N. Dandapat, B.K. Guha, S. Datta, D. Basu, "Synthesis and Characterisation of Freestanding Diamond Coatings", *Indian J. Eng. Mater. Sci.*, **20** (2013) 522–532.
47. Z. Nibennanoune, D. George, F. Antoni, S. Ahzi, D. Ruch, J. Gracio, Y. Remond, "Improving diamond coating on Ti6Al4V substrate using a diamond like carbon interlayer: Raman residual stress evaluation and AFM analyses", *Diam. Relat. Mater.*, **22** (2012) 105-12.
48. N. Ali, V.F. Neto, S. Mei, G. Cabral, Y. Kousar, E. Titus, A.A. Ogwu, D.S. Misra, J. Gracio, "Optimisation of the new time-modulated CVD process using the Taguchi method", *Thin Solid Films*, **469** (2004) 154–160.
49. U. Manju, M. Sreemony, A.K. Chakraborty, "Multitechnique photoelectron spectrometer for micro-area spectroscopy and imaging", *Curr. Sci.*, **105** [8] (2013) 1056–1060.
50. T.A. Grotjohn, J. Asmussen, "Microwave plasma-assisted diamond film deposition", pp. 211–302 in *Diamond Films Handbook*, Chapter 7, edited by J. Asmussen, D.K. Reinhard, Marcel Dekker, Inc., 2002.
51. S.S. Zuo, M.K. Yaran, T.A. Grotjohn, D.K. Reinhard, J. Asmussen, "Investigation of diamond deposition uniformity and quality for freestanding film and substrate applications", *Diam. Relat. Mater.*, **17** (2008) 300–305.
52. K. Kobashi, K. Nishimura, Y. Kawate, T. Horiuchi, "Synthesis of diamonds by use of microwave plasma chemical-vapor deposition: Morphology and growth of diamond films", *Phys. Rev. B*, **38** [6] (1988) 4067–4084.
53. A.K. Mallik, S. Bysakh, M. Sreemany, S. Roy, J. Ghosh, S. Roy, J.C. Mendes, J. Gracio, S. Datta, "Property mapping of polycrystalline diamond coatings over large area", *J. Adv. Ceram.*, **3** [1] (2014) 56–70.
54. Y. Fan, A.G. Fitzgerald, P. John, C.E Troupe, J.I.B. Wilson, "X-ray photoelectron spectroscopy studies of CVD diamond films", *Surf. Interface Anal.*, **34** (2002) 703–707.